ARTICLE IN PRESS

Available online at www.sciencedirect.com

SCIENCE DIRECT®

Physica A III (IIII) III–III

PHYSICA A

www.elsevier.com/locate/physa

Gaseous mixture flow between two parallel plates in the whole range of the gas rarefaction

S. Naris[a], D. Valougeorgis[a,*], D. Kalempa[b], F. Sharipov[b]

[a] *Department of Mechanical and Industrial Engineering, University of Thessaly, Pedion Areos, 38333 Volos, Greece*

[b] *Departamento de Física, Universidade Federal do Paraná, Caixa Postal 19044, 81531-990 Curitiba, Brazil*

Received 30 October 2003

Abstract

The flow of binary gaseous mixtures between two parallel plates driven by gradients of pressure, temperature and concentration is studied, based on the McCormack model of the Boltzmann equation. The coupled kinetic equations are solved numerically by the discrete velocity method. The mass flow, the heat flux and the diffusion flux, which are the mixture quantities of practical importance, are expressed in terms of the so-called thermodynamic fluxes. The latter are written in a form that allows us to verify the Onsager–Casimir reciprocity relations. In addition, analytical expressions for these quantities are derived in the limit case of the hydrodynamic regime. Thus, the numerical solution together with these expressions provides the solution in the whole range of the gas rarefaction. The influence of the intermolecular interaction potential is also investigated by comparing the results for the rigid sphere model with those for a realistic potential. Numerical results are presented for two binary mixtures of noble gases (Ne–Ar and He–Xe) for various values of the molar concentrations.

PACS: 47.45.−n; 44.15.+a; 47.45.Gx

Keywords: Rarefied gases; Mixtures; Knudsen number; Micro-fluidics

1. Introduction

Internal flows of rarefied gaseous mixtures caused by pressure, temperature and concentration gradients are of major importance in several applications in physics and

* Corresponding author.

E-mail addresses: snaris@mie.uth.gr (S. Naris), diva@mie.uth.gr (D. Valougeorgis), kalempa@fisica.ufpr.br (D. Kalempa), sharipov@fisica.ufpr.br (F. Sharipov).

0378-4371/$ - see front matter
doi:10.1016/j.physa.2003.12.047

engineering. The first two flows caused by pressure and temperature gradients arise even in single component gases and are known as the Poiseuille and thermal creep flow, respectively. The third flow corresponding to a concentration gradient occurs only in gaseous mixtures and it is known as the diffusion flow. Compared to the huge amount of papers in the case of a single gas [1–4], the available literature for gaseous mixtures is very limited.

Most of the existing works on gaseous mixtures are concentrated to an estimation of the viscous, thermal and diffusion slip coefficients studying the corresponding semi-infinite half-space problems. The fundamental theoretical significance and the great practical importance of the slip coefficients easily justify the interest in this area of research. It should be pointed out that the slip coefficients are important when the Knudsen number is moderately small ($0.1 < Kn < 0.001$) in order to provide suitable boundary conditions for the hydrodynamic equations. Previous calculations [5–9] have been based on the available, at that time, kinetic models for gaseous mixtures [10–12]. One of the major difficulties in dealing with gas mixtures is the large number of parameters, which are involved in the calculations. To deal with this situation, Ivchenco et al. [13,14] have developed recently, general and convenient expressions for the slip coefficients of various binary gas mixtures. More advanced calculations were carried out in the works [15,18] applying the McCormack model [19] and in the works [20,21] using the linearized Boltzman equation.

It should be noted that the renewed interest to internal rarefied flows has been motivated by the recent development in the micro-electro-mechanical systems (MEMS) technology. In most MEMS applications, the continuum equations are applied with the appropriate slip boundary conditions [22,23]. It is evident, however, that the approaches based on kinetic theory are more suitable to solve such type of the problems, since the whole range of the gas rarefaction can be studied in an uniform manner.

In spite of the great importance of the internal rarefied flows of gaseous mixtures there are very few articles in the literature concerning this topic. Numerical results for mixture flows through tubes and channels have been obtained in Ref. [24] by the variational method. The Couette flow for a gas mixture in a plane channel has been also solved in Ref. [25] using the discrete velocity method. More recently the flow of a gaseous mixture through a tube is studied based on the McCormack kinetic model [26], providing reliable results for the thermodynamic fluxes and the kinetic coefficients.

Nowadays, using the modern computers it becomes possible to solve the exact Boltzmann equation. However, the model kinetic equations continue to be a widely used computational tool in practical calculations because they provide reliable results with very modest computational efforts. To guarantee the reliability of results it is necessary to chose correctly the model equation among those proposed in numerous papers, see e.g. Refs. [10–12,19,27–29]. All these model equations satisfy the conservation laws and the H-theorem. However, a majority of them do not provide the correct expressions for all transport coefficients, i.e., viscosity, thermal conductivity, diffusion and thermal diffusion ratio. Thus, the McCormack model [19] seems to be most appropriate for our purpose because all transport coefficients can be obtained from it applying the Chapman–Enskog procedure. A comparison of the previous results based on this

model [16–18,30] with those obtained from the Boltzmann equation [20,21] confirmed the reliability of the McCormack model.

In the present work, this model is applied to solve the flow of binary gas mixtures between two parallel plates driven by gradients of pressure, temperature and concentration. The solution includes the investigation of direct and cross effects and it is complete and accurate for the whole range of the gas rarefaction. Numerical results for the mass, heat and diffusion fluxes are provided for two different mixtures. The influence of the intermolecular interaction law on the fluxes is also investigated using the rigid sphere model and a realistic potential based on experimental data. Analytical expressions for the fluxes are provided in the hydrodynamic limit.

2. Statement of the problem and definitions

Consider a binary gaseous mixture confined between two parallel plates fixed at $y' = \pm H/2$. The flow is caused by longitudinal small gradients of pressure, temperature and concentration defined as

$$X_P = \frac{H}{P}\frac{\partial P}{\partial x'}, \quad X_T = \frac{H}{T}\frac{\partial T}{\partial x'}, \quad X_C = \frac{H}{C}\frac{\partial C}{\partial x'}, \tag{1}$$

respectively. The smallness of the gradients means that

$$|X_P| \ll 1, \quad |X_T| \ll 1, \quad |X_C| \ll 1 . \tag{2}$$

Here, x' is the longitudinal coordinate, P, T and C are pressure, temperature and molar concentration of the mixture in a given cross section. The molar concentration C of the mixture is defined as

$$C = \frac{n_1}{n_1 + n_2}, \tag{3}$$

where n_α $(\alpha = 1, 2)$ is the number density of gaseous species α. Moreover, we neglect the end effects and consider only the longitudinal components of the hydrodynamic (bulk) velocity $\mathbf{u}'$ and heat flow vector $\mathbf{q}'$, which are functions only of the transverse coordinate y', i.e.,

$$\mathbf{u}' = (u'(y), 0, 0), \quad \mathbf{q}' = (q'(y), 0, 0) . \tag{4}$$

The quantities of practical interest include the mass flow rate, the heat flux and the diffusion flux given by

$$J_M = \int_{-H/2}^{H/2} \varrho u' \, \mathrm{d}y', \tag{5}$$

$$J_H = \int_{-H/2}^{H/2} q' \, \mathrm{d}y', \tag{6}$$

$$J_D = \int_{-H/2}^{H/2} \varrho_1 (u_1' - u') \, \mathrm{d}y' = \int_{-H/2}^{H/2} \frac{\varrho_1 \varrho_2}{\varrho} (u_1' - u_2') \, \mathrm{d}y', \tag{7}$$

respectively. Here, ϱ is the mass density of the mixture

$$\varrho = \varrho_1 + \varrho_2 \,, \tag{8}$$

$\varrho_\alpha = n_\alpha m_\alpha$ is the mass density of each species and m_α ($\alpha = 1,2$) denotes the molecular mass. The hydrodynamic velocity of the mixture is defined as

$$u' = \frac{1}{\varrho}(\varrho_1 u_1' + \varrho_2 u_2') \,, \tag{9}$$

where u_1' and u_2' are the bulk velocities of each species. It is also convenient to introduce the mean velocity of the mixture

$$w = \frac{1}{n}(n_1 u_1' + n_2 u_2') \tag{10}$$

and the so-called peculiar heat flow

$$q^* = q' - \frac{5}{2} P(w - u') \,. \tag{11}$$

The calculations are carried out in the whole range of the gas rarefaction parameter defined as

$$\delta = \frac{HP_0}{\mu}\sqrt{\frac{m}{2kT_0}} \,, \tag{12}$$

where P_0 and T_0 are the equilibrium pressure and temperature of the mixture, respectively, μ the stress viscosity coefficient of the mixture at the temperature T_0, k is the Boltzmann constant and m is the mean molecular mass of the mixture given by

$$m = C_0 m_1 + (1 - C_0) m_2 \tag{13}$$

with C_0 to denote the equilibrium molar concentration.

Owing to the smallness of the thermodynamic forces given in Eq. (2), the Boltzmann equation can be linearized by the standard manner representing the distribution function as

$$f_\alpha(x', y', \mathbf{v}_\alpha) = f_\alpha^0(x', \mathbf{v}_\alpha)[1 + h_\alpha(y', \mathbf{v}_\alpha)], \quad |h_\alpha| \ll 1 \,, \tag{14}$$

where

$$f_\alpha^0(x', \mathbf{v}_\alpha) = n_\alpha(x')\left[\frac{m_\alpha}{2\pi kT(x')}\right]^{3/2} \exp\left[-\frac{m_\alpha v_\alpha^2}{2kT(x')}\right] \tag{15}$$

is the local Maxwellian and $h_\alpha = h_\alpha(y', \mathbf{v}')$ is a perturbation function. Further, it is convenient to use the dimensionless molecular velocity $\mathbf{c}_\alpha$ ($\alpha = 1,2$) and the dimensionless coordinates x and y defined as

$$\mathbf{c}_\alpha = \sqrt{\frac{m_\alpha}{2kT_0}}\,\mathbf{v}_\alpha, \quad x = \frac{x'}{H}, \quad y = \frac{y'}{H} \,. \tag{16}$$

Then, the system of the two linearized Boltzmann equations reads

$$c_{\alpha y}\frac{\partial h_\alpha}{\partial y} = \omega_\alpha \sum_{\beta=1}^{2} L_{\alpha\beta} h_\alpha - c_{\alpha x}\left[X_P + \eta_\alpha X_C + \left(c_\alpha^2 - \frac{5}{2}\right) X_T\right], \quad \alpha = 1,2 \,, \tag{17}$$

where

$$\eta_1 = 1, \quad \eta_2 = -\frac{C_0}{(1-C_0)} \tag{18}$$

and

$$\omega_\alpha = H\sqrt{\frac{m_\alpha}{2kT_0}}\,. \tag{19}$$

The dimensionless moments of the perturbation function read as

$$u_\alpha(y) = \frac{1}{\pi^{3/2}}\sqrt{\frac{m}{m_\alpha}}\int c_{\alpha x} h_\alpha(y,\mathbf{c})\exp(-c_\alpha^2)\,\mathrm{d}\mathbf{c}_\alpha\,, \tag{20}$$

$$q_\alpha(y) = \frac{1}{\pi^{3/2}}\sqrt{\frac{m}{m_\alpha}}\int c_{\alpha x}\left(c_\alpha^2 - \frac{5}{2}\right) h_\alpha(y,\mathbf{c})\exp(-c_\alpha^2)\,\mathrm{d}\mathbf{c}_\alpha \tag{21}$$

and

$$\Pi_\alpha(y) = \pi^{-3/2}\int c_{\alpha x} c_{\alpha y} h_\alpha(y,\mathbf{c})\exp(-c_\alpha^2)\,\mathrm{d}\mathbf{c}_\alpha\,. \tag{22}$$

The dimensional quantities are expressed in terms of the dimensionless ones as

$$u'_\alpha = \sqrt{\frac{2kT_0}{m}}\,u_\alpha\,, \tag{23}$$

$$w = \sqrt{\frac{2kT_0}{m}}\,[C_0 u_1 + (1-C_0)u_2]\,, \tag{24}$$

$$q^* = P_0\sqrt{\frac{2kT_0}{m}}\,[C_0 q_1 + (1-C_0)q_2]\,. \tag{25}$$

In Eq. (17), the exact collision term $L_{\alpha\beta}$ has been replaced by the model proposed by McCormack [19], which is explicitly given in Appendix A for the problem under consideration. Using Eq. (12) and the definitions of Appendix A, it is easily seen that

$$\omega_\alpha = \delta\left[\frac{C_0}{\gamma_1} + \frac{1-C_0}{\gamma_2}\right]\sqrt{\frac{m_\alpha}{m}}\,, \tag{26}$$

where γ_α ($\alpha = 1,2$) are the collision frequencies given by Eq. (A.1).

Since Eq. (17) is linear its solution can be decomposed as

$$h_\alpha = h_\alpha^{(P)}X_P + h_\alpha^{(T)}X_T + h_\alpha^{(C)}X_C \tag{27}$$

and, consequently, the moments of the distribution function are also split into three independent parts:

$$u_\alpha = u_\alpha^{(P)}X_P + u_\alpha^{(T)}X_T + u_\alpha^{(C)}X_C\,, \tag{28}$$

$$q_\alpha = q_\alpha^{(P)}X_P + q_\alpha^{(T)}X_T + q_\alpha^{(C)}X_C\,, \tag{29}$$

$$\Pi_\alpha = \Pi_\alpha^{(P)}X_P + \Pi_\alpha^{(T)}X_T + \Pi_\alpha^{(C)}X_C\,. \tag{30}$$

Finally, the dimensionless velocity and heat flow profiles are integrated to yield the reduced mass flow rate

$$U_\alpha^{(i)} = -2\int_{-1/2}^{1/2} u_\alpha^{(i)}(y)\,\mathrm{d}y \tag{31}$$

and the heat flux

$$Q_\alpha^{(i)} = -2\int_{-1/2}^{1/2} q_\alpha^{(i)}(y)\,\mathrm{d}y \tag{32}$$

for $\alpha = 1,2$ and $i = P,T,C$.

We are going to solve Eq. (17) assuming diffuse boundary conditions, and to compute the velocity, heat flow and stress profiles as well as the mass and heat fluxes, given by Eqs. (31) and (32).

3. Thermodynamic analysis

A general thermodynamic analysis of many types of thermodynamic systems is given in the book [31], which is based on the local equilibrium principle, i.e., it is valid only in the hydrodynamic regime. Such an analysis allows us to obtain the Onsager–Casimir reciprocity relations and to reduce the number of kinetic coefficients needed to determine non-reversible phenomena. In Refs. [32–34] the Onsager–Casimir reciprocity relations were obtained in general form for rarefied gas flows without the local equilibrium principle, i.e., for the whole range of the gas rarefaction. In the case of gaseous mixture in a tube these relations are given in the paper [26]. Here we repeat only the key elements of this thermodynamic analysis properly modified for the case of the channel flow.

It has been shown that although the fluxes J_M, J_H and J_D, defined by Eqs. (5)–(7) linearly depend on the thermodynamic forces X_P, X_T and X_C the kinetic coefficients of these equations do not satisfy the Onsager–Casimir reciprocity relations. However, the reciprocity relations are fulfilled when the following thermodynamic fluxes are introduced [34]:

$$J_P = -n_0\int_{-H/2}^{H/2} w\,\mathrm{d}y' , \tag{33}$$

$$J_T = -\frac{1}{kT_0}\int_{-H/2}^{H/2} q^*\,\mathrm{d}y' , \tag{34}$$

$$J_C = -n_{01}\int_{-H/2}^{H/2} (u_1' - u_2')\,\mathrm{d}y' . \tag{35}$$

Then the thermodynamic fluxes are related to the thermodynamic forces in the matrix form

$$\begin{pmatrix} J_P \\ J_T \\ J_C \end{pmatrix} = \begin{pmatrix} \Lambda'_{PP} & \Lambda'_{PT} & \Lambda'_{PC} \\ \Lambda'_{TP} & \Lambda'_{TT} & \Lambda'_{TC} \\ \Lambda'_{CP} & \Lambda'_{CT} & \Lambda'_{CC} \end{pmatrix} \begin{pmatrix} X_P \\ X_T \\ X_C \end{pmatrix} . \tag{36}$$

Since all thermodynamic forces considered here do not change their own sing under the time reversal the Onsager–Casimir relations take the form

$$\Lambda'_{PT} = \Lambda'_{TP}, \quad \Lambda'_{PC} = \Lambda'_{CP}, \quad \Lambda'_{TC} = \Lambda'_{CT} \, . \tag{37}$$

All kinetic coefficients have the same dimension and for further derivations it is convenient to use the reduced kinetic coefficient in the form

$$\Lambda_{ij} = \frac{2}{n_0 H} \sqrt{\frac{m}{2kT_0}} \, \Lambda'_{ij} \, . \tag{38}$$

The coefficients Λ_{PP}, Λ_{TT} and Λ_{CC} corresponding to the Poiseuille flow, thermal conductivity and diffusion flux, respectively, describe the so-called direct effects, while the non-diagonal coefficients Λ_{ij} $(i \neq j)$ are related to the so-called cross effects.

Thus, once the set of coefficients Λ_{ij} $(i, j = P, T, C)$ is known, the fluxes J_P, J_T and J_C can be easily calculated via Eq. (36). Then, the fluxes J_M, J_H and J_D, which are of practical interest, can be deduced from the expressions

$$J_M = -mJ_P + (m_2 - m_1)(1 - C_0)J_C \, , \tag{39}$$

$$J_H = -kT_0 \left[J_T + \frac{5}{2} \frac{m_2 - m_1}{m} (1 - C_0) J_C \right] \, , \tag{40}$$

$$J_D = -\frac{m_1 m_2}{m} (1 - C_0) J_C \, . \tag{41}$$

At this stage it is important to express the reduced kinetic coefficients Λ_{ij} $(i, j = P, T, C)$ in terms of the reduced mass flow and heat flux given by Eqs. (31) and (32). After some algebraic manipulation, combining Eqs. (33)–(35) with Eqs. (10), (11), (28) and (29) we find

$$\Lambda_{Pi} = C_0 U_1^{(i)} + (1 - C_0) U_2^{(i)} \, , \tag{42}$$

$$\Lambda_{Ti} = C_0 Q_1^{(i)} + (1 - C_0) Q_2^{(i)} \, , \tag{43}$$

$$\Lambda_{Ci} = C_0 [U_1^{(i)} - U_2^{(i)}] \, , \tag{44}$$

where $i = P$, T, C. Thus, the total number of the nine unknowns is reduced down to six due to the application of the Onsager–Casimir relations.

4. Hydrodynamic regime

In the hydrodynamic regime, the Navier–Stokes equation with the viscous [16], thermal [17] and diffusion [18] slip coefficients provides the following velocity profile for the problem under question

$$u' = -\frac{P_0 H}{2\mu} \left(\frac{1}{4} - y^2 + \frac{\sigma_P}{\delta} \right) X_P + \frac{\mu}{HQ} (\sigma_T X_T + \sigma_C X_C) \, . \tag{45}$$

To calculate the heat and diffusion flows the Fourier and Fick equations are applied. According to the first Chapman–Enskog approximation [1] we have

$$q^* = -\kappa \frac{T_0}{H} X_T + P_0 C_0 (1 - C_0) \alpha_T (u_1' - u_2') \,, \tag{46}$$

$$u_1' - u_2' = -\frac{D_{12}}{H} \left[\frac{m_2 - m_1}{m} X_P + \alpha_T X_T + \frac{1}{1 - C_0} X_C \right] \,, \tag{47}$$

where κ is the heat conductivity, D_{12} is the diffusion coefficient and α_T is the thermal diffusion ratio. The expressions of the transport coefficients μ, κ, D_{12} and α_T are given in Ref. [26]. Note that in front of the right-hand side of Eq. (73) in Ref. [26], a minus sign has been omitted by mistake. The slip coefficients σ_P, σ_T and σ_C based on the McCormack kinetic model are given in Refs. [16–18], respectively. As it is known Eqs. (46) and (47) are not complete because some first order terms with respect to the Knudsen number, i.e., $O(1/\delta)$, appear in the second-order Chapman–Enskog approximation. Moreover, the heat and diffusion flows in the Knudsen layer also have terms of the first order. So, if one obtains the coefficients Λ_{CP} and Λ_{TP} from Eqs. (46) and (47), they will not satisfy the reciprocity relations given by Eqs. (37). However, since Eq. (45) contains all terms of $O(1/\delta)$ we obtain the coefficients Λ_{PC} and Λ_{PT} and then the coefficients Λ_{CP} and Λ_{TP} are calculated from Eqs. (37). Following this procedure, and after some considerable algebra the kinetic coefficients in the continuum limit read

$$\Lambda_{PP} = \frac{\delta}{6} + \sigma_P \tag{48}$$

$$\Lambda_{TT} = \frac{\varrho}{\mu} \left[\kappa \frac{T_0}{P_0} + C_0 (1 - C_0) \alpha_T^2 D_{12} \right] \frac{1}{\delta} \,, \tag{49}$$

$$\Lambda_{CC} = \frac{C_0 \varrho D_{12}}{(1 - C_0)\mu} \frac{1}{\delta} \,, \tag{50}$$

$$\Lambda_{PC} = \Lambda_{CP} = \left[\frac{n_{01} D_{12}}{\mu} (m_2 - m_1) - \sigma_C \right] \frac{1}{\delta} \,, \tag{51}$$

$$\Lambda_{PT} = \Lambda_{TP} = \left[\frac{n_{01} (1 - C_0) D_{12} \alpha_T}{\mu} (m_2 - m_1) - \sigma_T \right] \frac{1}{\delta} \,, \tag{52}$$

$$\Lambda_{TC} = \Lambda_{CT} = \frac{n_{01} m D_{12} \alpha_T}{\mu} \frac{1}{\delta} \,. \tag{53}$$

Eqs. (48)–(53) represent a complete set of closed-form expressions for the unknown kinetic coefficients at the hydrodynamic limit.

5. The numerical scheme

Since the flow is one-dimensional and fully developed in the longitudinal direction x, it is convenient to eliminate the $c_{\alpha x}$ and $c_{\alpha z}$ components ($\alpha = 1, 2$) of the molecular

velocity by introducing the functions

$$\Phi_\alpha(y,c_{\alpha y})=\frac{1}{\pi}\sqrt{\frac{m}{m_\alpha}}\int_{-\infty}^{\infty}\int_{-\infty}^{\infty}h_\alpha(y,\mathbf{c}_\alpha)c_{\alpha x}\mathrm{e}^{-c_{\alpha x}^2-c_{\alpha z}^2}\,\mathrm{d}c_{\alpha x}\,\mathrm{d}c_{\alpha z} \tag{54}$$

and

$$\Psi_\alpha(y,c_{\alpha y})=\frac{1}{\pi}\sqrt{\frac{m}{m_\alpha}}\int_{-\infty}^{\infty}\int_{-\infty}^{\infty}h_\alpha(y,\mathbf{c}_\alpha)c_{\alpha x}(c_{\alpha x}^2+c_{\alpha z}^2-2)\times\mathrm{e}^{-c_{\alpha x}^2-c_{\alpha z}^2}\,\mathrm{d}c_{\alpha x}\,\mathrm{d}c_{\alpha z}\ . \tag{55}$$

Eq. (17) is multiplied by the functions

$$\phi_\alpha(c_{\alpha x},c_{\alpha z})=\frac{1}{\pi}\sqrt{\frac{m}{m_\alpha}}\,c_{\alpha x}\mathrm{e}^{-c_{\alpha x}^2-c_{\alpha z}^2} \tag{56}$$

and

$$\psi_\alpha(c_{\alpha x},c_{\alpha z})=\frac{1}{\pi}\sqrt{\frac{m}{m_\alpha}}\,c_{\alpha x}(c_{\alpha x}^2+c_{\alpha z}^2-2)\mathrm{e}^{-c_{\alpha x}^2-c_{\alpha z}^2} \tag{57}$$

successively and the resulting equations are integrated with respect to $c_{\alpha x}$ and $c_{\alpha z}$. From these projections we find a set of four coupled integro-differential equations written as

$$\begin{aligned}c_{\alpha y}\frac{\partial\Phi_\alpha}{\partial y}+\omega_\alpha\gamma_\alpha\Phi_\alpha=&-\frac{1}{2}\sqrt{\frac{m}{m_\alpha}}\left[X_P+\eta_\alpha X_C+\left(c_{\alpha y}^2-\frac{1}{2}\right)X_T\right]\\&+\omega_\alpha\left\{\gamma_\alpha u_\alpha-\nu_{\alpha\beta}^{(1)}(u_\alpha-u_\beta)-\frac{1}{2}\,\nu_{\alpha\beta}^{(2)}\left(q_\alpha-\frac{m_\alpha}{m_\beta}\,q_\beta\right)\right.\\&+2\sqrt{\frac{m}{m_\alpha}}[(\gamma_\alpha-\nu_{\alpha\alpha}^{(3)}+\nu_{\alpha\alpha}^{(4)}-\nu_{\alpha\beta}^{(3)})\Pi_\alpha+\nu_{\alpha\beta}^{(4)}\Pi_\beta]c_{\alpha y}\\&+\frac{2}{5}\left[(\gamma_\alpha-\nu_{\alpha\alpha}^{(5)}+\nu_{\alpha\alpha}^{(6)}-\nu_{\alpha\beta}^{(5)})q_\alpha+\nu_{\alpha\beta}^{(6)}\sqrt{\frac{m_\beta}{m_\alpha}}\,q_\beta\right.\\&\left.\left.-\frac{5}{4}\,\nu_{\alpha\beta}^{(2)}(u_\alpha-u_\beta)\right]\left(c_{\alpha y}^2-\frac{1}{2}\right)\right\},\quad\alpha=1,2,\quad\beta\neq\alpha\ ,\end{aligned} \tag{58}$$

and

$$\begin{aligned}c_{\alpha y}\frac{\partial\Psi_\alpha}{\partial h}+\omega_\alpha\gamma_\alpha\Psi_\alpha=&-\sqrt{\frac{m}{m_\alpha}}\,X_T+\omega_\alpha\,\frac{4}{5}\left[(\gamma_\alpha-\nu_{\alpha\alpha}^{(5)}+\nu_{\alpha\alpha}^{(6)}-\nu_{\alpha\beta}^{(5)})q_\alpha\right.\\&\left.+\nu_{\alpha\beta}^{(6)}\sqrt{\frac{m_\beta}{m_\alpha}}\,q_\beta-\frac{5}{4}\,\nu_{\alpha\beta}^{(2)}(u_\alpha-u_\beta)\right],\quad\alpha=1,2,\quad\beta\neq\alpha\ ,\end{aligned} \tag{59}$$

where

$$u_\alpha(y) = \frac{1}{\sqrt{\pi}} \int_{-\infty}^{\infty} \Phi_\alpha e^{-c_{\alpha y}^2} \, dc_{\alpha y} \, , \tag{60}$$

$$q_\alpha(y) = \frac{1}{\sqrt{\pi}} \int_{-\infty}^{\infty} \left[\Psi_\alpha + \left(c_{\alpha y}^2 - \frac{1}{2} \right) \Phi_\alpha \right] e^{-c_{\alpha y}^2} \, dc_{\alpha y} \, , \tag{61}$$

$$\Pi_\alpha(y) = \frac{1}{\sqrt{\pi}} \sqrt{\frac{m_\alpha}{m}} \int_{-\infty}^{\infty} \Phi_\alpha c_{\alpha y} e^{-c_{\alpha y}^2} \, dc_{\alpha y} \, . \tag{62}$$

The discretization in the phase space is performed using the discrete velocity method (DVM). The roots of the Hermite polynomial of order N is chosen to define the set of discrete molecular velocities $c_{\alpha y}^n$, $n = 1, 2, \ldots, N$, and all integrals are approximated using the corresponding Gauss–Hermite quadratures. The discretization in the physical space is implemented by the so-called diamond-difference (DD) scheme [35]. The slab is divided in K intervals and then Eqs. (58) and (59) are discretized at the center of each interval $k = 1, 2, \ldots, K$. The first derivatives are approximated by centered finite differences, while all other terms are expressed in terms of the corresponding quantities at the edges of each interval using weighted averages. When the weights are equal the scheme is known as the DD scheme. As a result the spatial discretization is second-order accurate.

As it is well known, when the rarefaction parameter is large the convergence rate of the DVM is slow. Also, the large number of iterations does not always improve the accuracy of the results, since it may result to accumulated round-off error. In these cases an accelerated algorithm of the DVM is implemented to reduce significantly the required number of iterations and ensure accurate results [36]. In addition an optimized version of the DVM is used in the hydrodynamic limit to reduce the required number of grid points [37]. Both improvements reduce significantly the required CPU time and are particularly important in multi-dimensional problems [30].

6. Results and discussion

The results presented here, are based on the numerical scheme described in the previous section. Their convergence has been extensively examined, by modifying the number of discrete velocities and grid points. The tabulated results have converged to all figures shown and they are based on a 128 point Gauss–Hermite quadrature to simulate the velocity space and on a discretization of 101 grid points ($\Delta h = 10^{-2}$) to approximate the physical space. The relative convergence criterion is 10^{-6}. The accuracy of the numerical results has also been verified in several other ways. In all cases tested, we have seen that our results confirm the Onsager–Casimir reciprocity relations listed in Eq. (37) to many significant figures. Also, when we allow our data to reduce to the case of a single gas by taking $m_1 = m_2$, $d_1 = d_2$, the known results of the S model [38], are recovered. Finally, by comparing our results with the analytical results in the hydrodynamic limits, obtained by Eqs. (48)–(53), we have found that

the asymptotic behavior of our numerical solution in this limit is correct. All these verifications have been performed by two different computer codes, implementing the typical discrete velocity method and its accelerated version.

The numerical results presented here refer to the gaseous mixtures of Ne–Ar and He–Xe. The molecular masses of these species are $m_{Ne} = 20.183$, $m_{Ar} = 39.948$, $m_{He} = 4.0026$ and $m_{Xe} = 131.3$ in atomic units. Thus, the study includes one mixture with particles of about equal masses and another one with particles of very different masses.

To study the influence of the intermolecular interaction potential upon the kinetic coefficients two molecular models are used: the rigid spheres and a realistic potential of the intermolecular interaction. In the case of the rigid spheres the molecular diameters d_α of every species α are calculated via the expression obtained in Refs. [39,40]

$$\mu_\alpha = 1.016034\,\frac{5}{16}\,\frac{\sqrt{\pi m_\alpha kT}}{\pi d_\alpha^2} \tag{63}$$

and the experimental data on the viscosities μ_α of the single gases He, Ne, Ar and Xe at the temperature $T = 300$ K given in Ref. [41]. The diameter ratios d_2/d_1 are taken equal to 1.406 and 2.226 for the mixtures Ne–Ar and He–Xe, respectively. For the realistic potential the omega integrals are calculated using the expressions given in Ref. [41] assuming the same temperature as that for the rigid spheres, i.e., $T = 300$ K. These expressions of the omega integrals reproduce all transport coefficients for the mixtures within the experimental error.

The reduced kinetic coefficients Λ_{ij}, $(i, j = P, T, C)$, for the two mixtures under investigation are tabulated in Tables 1–6. The computations have been carried out for the wide range of the rarefaction parameter δ $(10^{-3} \leqslant \delta \leqslant 10^2)$ and for three values of the molar concentration $C_0 = 0.1$, 0.5 and 0.9. Also, in Table 7, the coefficients Λ_{ij}, $(i, j = P, T, C)$ obtained from Eqs. (48)–(53), which are valid in the hydrodynamic limit $(\delta \to \infty)$, are given.

Table 1
Kinetic coefficients vs. the gas rarefaction δ for the Ne–Ar mixture with $C_0 = 0.1$

δ	Λ_{PP}	Λ_{TT}	Λ_{CC}	$-\Lambda_{TP} = -\Lambda_{PT}$	$\Lambda_{CP} = \Lambda_{PC}$	$-\Lambda_{CT} = -\Lambda_{TC}$
Rigid spheres						
1.0 (−3)	4.3447	9.7492	6.4513 (−1)	1.8873	1.8428 (−1)	8.1291 (−2)
1.0 (−2)	3.1034	6.8492	4.5540 (−1)	1.2688	1.3247 (−1)	5.6814 (−2)
1.0 (−1)	2.0720	4.1235	2.7329 (−1)	7.4568 (−1)	8.0588 (−2)	3.5950 (−2)
1.0	1.5687	1.7789	1.1282 (−1)	3.7077 (−1)	3.2054 (−2)	1.9736 (−2)
1.0 (1)	2.7873	3.4517 (−1)	1.9851 (−2)	9.9167 (−2)	5.0455 (−3)	4.5728 (−3)
1.0 (2)	1.7696 (1)	3.7667 (−2)	2.1184 (−3)	1.1678 (−2)	5.2409 (−4)	5.0614 (−4)
Realistic potential						
1.0 (−3)	4.3453	9.7505	6.4668 (−1)	1.8875	1.8581 (−1)	8.1919 (−2)
1.0 (−2)	3.1039	6.8511	4.5746 (−1)	1.2690	1.3398 (−1)	5.6872 (−2)
1.0 (−1)	2.0725	4.1272	2.7706 (−1)	7.4553 (−1)	8.2050 (−2)	3.4078 (−2)
1.0	1.5690	1.7848	1.1856 (−1)	3.7046 (−1)	3.3021 (−2)	1.5421 (−2)
1.0 (1)	2.7878	3.4757 (−1)	2.1980 (−2)	9.9420 (−2)	4.9308 (−3)	2.8686 (−3)
1.0 (2)	1.7697 (1)	3.7961 (−2)	2.3673 (−3)	1.1727 (−2)	4.9367 (−4)	3.0279 (−4)

Table 2
Kinetic coefficients vs. the gas rarefaction δ for the Ne–Ar mixture with $C_0 = 0.5$

δ	Λ_{PP}	Λ_{TT}	Λ_{CC}	$-\Lambda_{TP} = -\Lambda_{PT}$	$\Lambda_{CP} = \Lambda_{PC}$	$-\Lambda_{CT} = -\Lambda_{TC}$
Rigid spheres						
1.0 (−3)	4.4871	1.0069 (1)	4.4730	1.9502	8.1505 (−1)	3.5955 (−1)
1.0 (−2)	3.2072	7.0807	3.1365	1.3128	5.8409 (−1)	2.5149 (−1)
1.0 (−1)	2.1371	4.2620	1.8589	7.7176 (−1)	3.5201 (−1)	1.6092 (−1)
1.0	1.5996	1.8305	7.4601 (−1)	3.8123 (−1)	1.3514 (−1)	8.9259 (−2)
1.0 (1)	2.8052	3.5491 (−1)	1.2603 (−1)	1.0133 (−1)	2.0280 (−2)	2.0031 (−2)
1.0 (2)	1.7712 (1)	3.8768 (−2)	1.3357 (−2)	1.1965 (−2)	2.1005 (−3)	2.2052 (−3)
Realistic potential						
1.0 (−3)	4.4870	1.0069 (1)	4.4740	1.9501	8.1457 (−1)	3.5861 (−1)
1.0 (−2)	3.2071	7.0825	3.1423	1.3125	5.8416 (−1)	2.4797 (−1)
1.0 (−1)	2.1373	4.2692	1.8800	7.7062 (−1)	3.5395 (−1)	1.4870 (−1)
1.0	1.5999	1.8444	7.8372 (−1)	3.7999 (−1)	1.3815 (−1)	6.6998 (−2)
1.0 (1)	2.8053	3.6047 (−1)	1.3882 (−1)	1.0187 (−1)	1.9870 (−2)	1.2030 (−2)
1.0 (2)	1.7712 (1)	3.9437 (−2)	1.4819 (−2)	1.2066 (−2)	1.9990 (−3)	1.2688 (−3)

Table 3
Kinetic coefficients vs. the gas rarefaction δ for the Ne–Ar mixture with $C_0 = 0.9$

δ	Λ_{PP}	Λ_{TT}	Λ_{CC}	$-\Lambda_{TP} = -\Lambda_{PT}$	$\Lambda_{CP} = \Lambda_{PC}$	$-\Lambda_{CT} = -\Lambda_{TC}$
Rigid spheres						
1.0 (−3)	4.3585	9.7803	2.9107 (1)	1.8934	1.2469	5.5008 (−1)
1.0 (−2)	3.1133	6.8715	2.0194 (1)	1.2730	8.8891 (−1)	3.8520 (−1)
1.0 (−1)	2.0781	4.1368	1.1729 (1)	7.4812 (−1)	5.2735 (−1)	2.5042 (−1)
1.0	1.5723	1.7845	4.4955	3.7157 (−1)	1.9109 (−1)	1.4014 (−1)
1.0 (1)	2.7914	3.4649 (−1)	7.1414 (−1)	9.9462 (−2)	2.7081 (−2)	3.0258 (−2)
1.0 (2)	1.7700 (1)	3.7817 (−2)	7.4973 (−2)	1.1720 (−2)	2.8044 (−3)	3.3117 (−3)
Realistic potential						
1.0 (−3)	4.3578	9.7787	2.9213 (1)	1.8930	1.2345	5.4249 (−1)
1.0 (−2)	3.1127	6.8706	2.0333 (1)	1.2726	8.7892 (−1)	3.7339 (−1)
1.0 (−1)	2.0779	4.1381	1.1964 (1)	7.4742 (−1)	5.2509 (−1)	2.2465 (−1)
1.0	1.5722	1.7886	4.8040	3.7102 (−1)	1.9714 (−1)	1.0067 (−1)
1.0 (1)	2.7907	3.4806 (−1)	8.0466 (−1)	9.9585 (−2)	2.7400 (−2)	1.7437 (−2)
1.0 (2)	1.7699 (1)	3.8002 (−2)	8.5091 (−2)	1.1741 (−2)	2.7743 (−3)	1.8383 (−3)

The negative sign at some of the kinetic coefficients, corresponding to cross effects, imply that in these cases there is a mass flow or a heat flux opposite to the main flow or flux due to the imposed thermodynamic force (gradient). For example, the negative sign in front of Λ_{PT} and Λ_{CT}, imply that there is flow caused by the temperature gradient, from a lower to a higher temperature, known as thermal creep and thermal diffusion (or Soret effect) flows, respectively.

For all cases considered here Λ_{PP} has the so-called Knudsen minimum at ($Kn \sim 1$), while all other coefficients are decreased when the rarefaction parameter δ is increased.

Table 4
Kinetic coefficients vs. the gas rarefaction δ for the He–Xe mixture with $C_0 = 0.1$

δ	Λ_{PP}	Λ_{TT}	Λ_{CC}	$-\Lambda_{TP} = -\Lambda_{PT}$	$\Lambda_{CP} = \Lambda_{PC}$	$-\Lambda_{CT} = -\Lambda_{TC}$
Rigid spheres						
1.0 (−3)	6.1070	1.3711 (1)	2.4824	2.6612	2.0307	8.9070 (−1)
1.0 (−2)	4.3703	9.6813	1.7710	1.8010	1.4530	6.1063 (−1)
1.0 (−1)	2.8593	5.8247	1.0868	1.0605	8.9365 (−1)	3.6299 (−1)
1.0	1.9267	2.4557	4.7538 (−1)	5.1259 (−1)	3.8871 (−1)	1.6808 (−1)
1.0 (1)	2.8820	4.7045 (−1)	9.2012 (−2)	1.2896 (−1)	7.3750 (−2)	3.4461 (−2)
1.0 (2)	1.7736 (1)	5.1425 (−2)	1.0008 (−2)	1.5045 (−2)	7.9721 (−3)	3.7634 (−3)
Realistic potential						
1.0 (−3)	6.1456	1.3800 (1)	2.5232	2.6801	2.0715	9.1041 (−1)
1.0 (−2)	4.4088	9.7807	1.8132	1.8180	1.4943	6.2762 (−1)
1.0 (−1)	2.8981	5.9572	1.1343	1.0710	9.3699 (−1)	3.7077 (−1)
1.0	1.9622	2.6120	5.2821 (−1)	5.1558 (−1)	4.3168 (−1)	1.6443 (−1)
1.0 (1)	2.8951	5.2953 (−1)	1.1353 (−1)	1.3108 (−1)	8.8919 (−2)	3.1817 (−2)
1.0 (2)	1.7739 (1)	5.8759 (−2)	1.2636 (−2)	1.5441 (−2)	9.7205 (−3)	3.3798 (−3)

Table 5
Kinetic coefficients vs. the gas rarefaction δ for the He–Xe mixture with $C_0 = 0.5$

δ	Λ_{PP}	Λ_{TT}	Λ_{CC}	$-\Lambda_{TP} = -\Lambda_{PT}$	$\Lambda_{CP} = \Lambda_{PC}$	$-\Lambda_{CT} = -\Lambda_{TC}$
Rigid spheres						
1.0 (−3)	1.0844 (1)	2.4360 (1)	1.0833 (1)	4.7462	7.7122	3.3852
1.0 (−2)	7.8049	1.7358 (1)	7.7462	3.2467	5.5364	2.3294
1.0 (−1)	5.0465	1.0539 (1)	4.8018	1.9278	3.4447	1.4007
1.0	3.0158	4.4534	2.1872	9.1884 (−1)	1.5625	6.7512 (−1)
1.0 (1)	3.2652	8.7344 (−1)	4.4886 (−1)	2.2321 (−1)	3.1405 (−1)	1.4608 (−1)
1.0 (2)	1.7955 (1)	9.6574 (−2)	4.9343 (−2)	2.6175 (−2)	3.4287 (−2)	1.6087 (−2)
Realistic potential						
1.0 (−3)	10.909 (1)	2.4512 (1)	1.0899 (1)	4.7773	7.7831	3.4182
1.0 (−2)	7.8720	1.7541 (1)	7.8236	3.2739	5.6125	2.3543
1.0 (−1)	5.1240	1.0830 (1)	4.9192	1.9405	3.5411	1.3968
1.0	3.1057	4.8564	2.3691	9.1427 (−1)	1.6882	6.3291 (−1)
1.0 (1)	3.3024	1.0386	5.3403 (−1)	2.2543 (−1)	3.6447 (−1)	1.2377 (−1)
1.0 (2)	1.7966 (1)	1.1732 (−1)	5.9880 (−2)	2.6926 (−2)	4.0148 (−2)	1.3112 (−2)

This behavior is similar to the single gas case. In the hydrodynamic regime, i.e., for large values of δ, the numerical values of the coefficient Λ_{PP} tend to those calculated by Eq. (48). All other kinetic coefficients Λ_{ij}, $(i, j = P, T, C)$ approach to the corresponding ones, given in Table 7. In particular, for $\delta = 100$, in most cases there is an agreement at least up to two significant figures.

The dependence of the results on the choice of the intermolecular interaction potential is studied, by comparing the corresponding results given in Tables 1–6, for the rigid

Table 6
Kinetic coefficients vs. the gas rarefaction δ for the He–Xe mixture with $C_0 = 0.9$

δ	Λ_{PP}	Λ_{TT}	Λ_{CC}	$-\Lambda_{TP} = -\Lambda_{PT}$	$\Lambda_{CP} = \Lambda_{PC}$	$-\Lambda_{CT} = -\Lambda_{TC}$
Rigid spheres						
1.0 (−3)	8.3897	1.8842 (1)	2.0977 (1)	3.6684	6.8039	2.9814
1.0 (−2)	6.0517	1.3434 (1)	1.4964 (1)	2.5081	4.8737	2.0480
1.0 (−1)	3.9984	8.2473	9.3289	1.4968	3.0633	1.2513
1.0	2.6609	3.6657	4.4633	7.4169 (−1)	1.4885	6.4810 (−1)
1.0 (1)	3.3488	7.6774 (−1)	9.8977 (−1)	2.0137 (−1)	3.3468 (−1)	1.4860 (−1)
1.0 (2)	1.8109 (1)	8.5864 (−2)	1.1022 (−1)	2.4422 (−2)	3.7385 (−2)	1.6410 (−2)
Realistic potential						
1.0 (−3)	8.3444	1.8740 (1)	2.1058 (1)	3.6454	6.7448	2.9494
1.0 (−2)	6.0122	1.3347 (1)	1.5065 (1)	2.4862	4.8264	2.0110
1.0 (−1)	3.9790	8.2093	9.5047	1.4768	3.0581	1.1946
1.0	2.6827	3.7005	4.7820	7.2377 (−1)	1.5686	5.6157 (−1)
1.0 (1)	3.3706	7.8756 (−1)	1.1645	1.9279 (−1)	3.9485 (−1)	1.0659 (−1)
1.0 (2)	1.8111 (1)	8.8275 (−2)	1.3235 (−1)	2.3187 (−2)	4.5275 (−2)	1.1023 (−2)

Table 7
Kinetic coefficients in the hydrodynamic regime computed by Eqs. (49)–(53)

C_0	Ne–Ar			He–Xe		
	0.1	0.5	0.9	0.1	0.5	0.9
Rigid spheres						
$\delta\Lambda_{TT}$	3.8018	3.9134	3.8170	5.1916	9.7619	8.6891
$\delta\Lambda_{CC}$	0.2134	1.3441	7.5348	1.0099	4.9843	11.148
$\delta\Lambda_{PC}$	0.0529	0.2108	0.2811	0.8038	3.4614	3.7819
$-\delta\Lambda_{TC}$	0.0512	0.2228	0.3343	0.3799	1.6253	1.6583
$-\delta\Lambda_{PT}$	1.1880	1.2172	1.1928	1.5291	2.6621	2.4926
Realistic potential						
$\delta\Lambda_{TT}$	3.8318	3.9815	3.8358	5.9413	11.884	8.9347
$\delta\Lambda_{CC}$	0.2386	1.4922	8.5606	1.2779	6.0606	13.413
$\delta\Lambda_{PC}$	0.0498	0.1995	0.2776	0.9818	4.0560	4.5922
$-\delta\Lambda_{TC}$	0.0305	0.1276	0.1849	0.3401	1.3191	1.1061
$-\delta\Lambda_{PT}$	1.1933	1.2279	1.1945	1.5716	2.7441	2.3645

sphere and the realistic potential cases. First, it is clearly seen that the coefficient Λ_{PP} is practically insensitive to the intermolecular potentials, while the coefficients Λ_{TT} and Λ_{PT} or (Λ_{TP}) are slightly sensitive to the potential in most cases studied here. From the other hand, the discrepancy in the values of Λ_{CC}, Λ_{CT} or (Λ_{TC}) and Λ_{CP} or (Λ_{PC}) for the two potentials become significant, particularly when $\delta > 10^{-1}$. Thus, the implementation of the rigid sphere model in the two gaseous mixtures tested here, provide accurate results for the four among the nine reduced kinetic coefficients

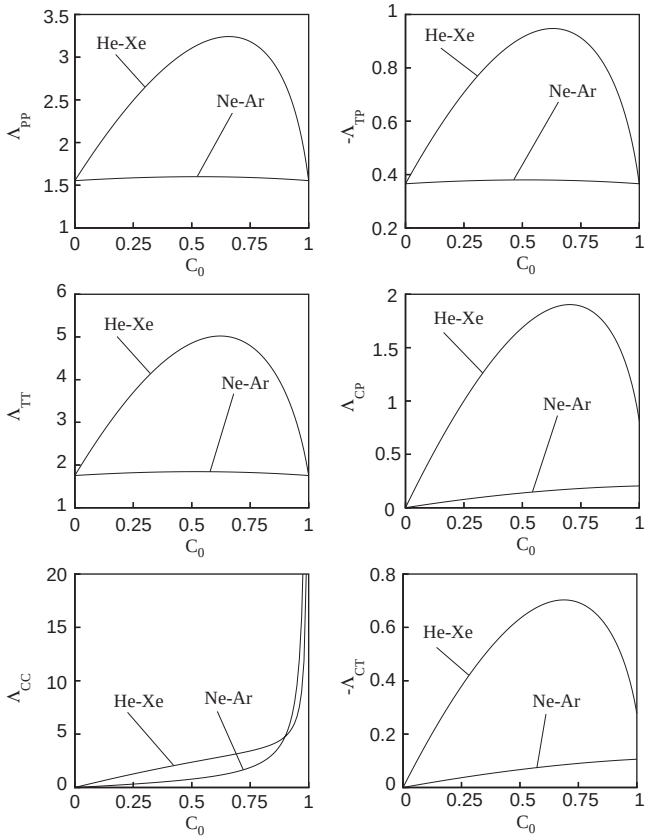

Fig. 1. Kinetic coefficients vs. the concentration C_0 for $\delta = 1$ and realistic potential.

involved. As a consequence, it may be concluded that the rigid sphere model should be avoided in gaseous mixture flows, particularly when the diffusion flow problem is studied. It may be also stated that the effect of the intermolecular interaction potential is more dominant in the He–Xe mixture rather than in the Ne–Ar mixture.

The behavior of the kinetic coefficients in terms of the molar concentration C_0 for both mixtures and $\delta = 1$ is shown in Fig. 1. It is useful to remind that, due to the definition of the molar concentration, higher values of C_0 correspond to higher values of n_1, which is taken always to be the lighter species. As it was expected the variation of C_0 has a much more significant effect on the results of the He–Xe mixture, which has a larger ratio of the molecular masses than the Ne–Ar mixture. Actually, the coefficients Λ_{PP}, Λ_{TT} and Λ_{PT} or (Λ_{TP}) have a small variation for $0 \leqslant C_0 \leqslant 1$. The coefficient Λ_{CC} is the one with the most strong dependency on C_0 and it increases by increasing the concentration of the lighter component. Note, the values of the kinetic coefficients Λ_{CC}, Λ_{CP} (or Λ_{PC}) and Λ_{CT} (or Λ_{TC}) at $C_0 = 1$ must be considered as limit values because the concentration $C_0 = 1$ means that the first component of the

mixture is single and the corresponding phenomena do not exist. In other words, the limit values correspond to the concentration very close to unity but not equal to unity. The behavior of the Λ_{ij} in terms of C_0, shown in Fig. 1 for $\delta = 1$, is similar for other values of δ. The main difference is that as δ increases, the value of the concentration where the peak values of the Λ_{ij} occurs, moves from left to right (from zero to one).

Finally, the velocity profiles of each species of the two mixtures are presented in Figs. 2–7, for $\delta = 0.1, 1$ and 10 and for $C_0 = 0.1, 0.5$ and 0.9. For $\delta = 0.1$ and 1 the velocities of each component are different. For $\delta = 10$ the velocities are parabolic and almost equal to each other that corresponds to the hydrodynamic solution. When the flow is due to pressure or temperature gradients the lighter component has always the higher velocity even near the hydrodynamic regime. When the flow is due to a concentration gradient the velocities of each component have the opposite directions. In this case, for small values of C_0 the light particles have higher, but for high values of C_0 it is the other way around.

7. Concluding remarks

The flow of binary gaseous mixtures between two parallel plates driven by gradients of pressure, temperature and concentration has been studied on the bases of the McCormack model. The solution is complete in the sense that it includes the investigation of both direct and cross effects and it is accurate for the whole range of the gas rarefaction. Numerical results are presented for two binary mixtures of noble gases (Ne–Ar and He–Xe) with various values of the molar concentration. The results include velocity profiles across the channel of each component of the two mixtures and the so-called reduced kinetic coefficients, which satisfy Onsager–Casimir reciprocity relations. Then the overall quantities, which are important for engineering purposes, are deduced. Analytical expressions for the kinetic coefficients at the hydrodynamic limit have been derived. The influence of the intermolecular interaction potential is also investigated by comparing the results for the rigid sphere model with those of a realistic potential, based on an experimental data. It has been concluded that the rigid sphere model should be avoided in gaseous mixture flows particularly when the diffusion flow problem is studied. The present work provides a better understanding and some helpful knowledge on the gaseous mixture behavior in terms of several parameters, such as molecular masses and diameters ratios of the species, molar concentration, intermolecular interaction laws and rarefaction parameter.

Acknowledgements

The partial support of this work by the Association EURATOM-Hellenic Republic (Contract ERB 5005 CT 990100) and the Conselho Nacional de Desenvolvimento Científico e Tecnológico (CNPq, Brazil) is gratefully acknowledged.

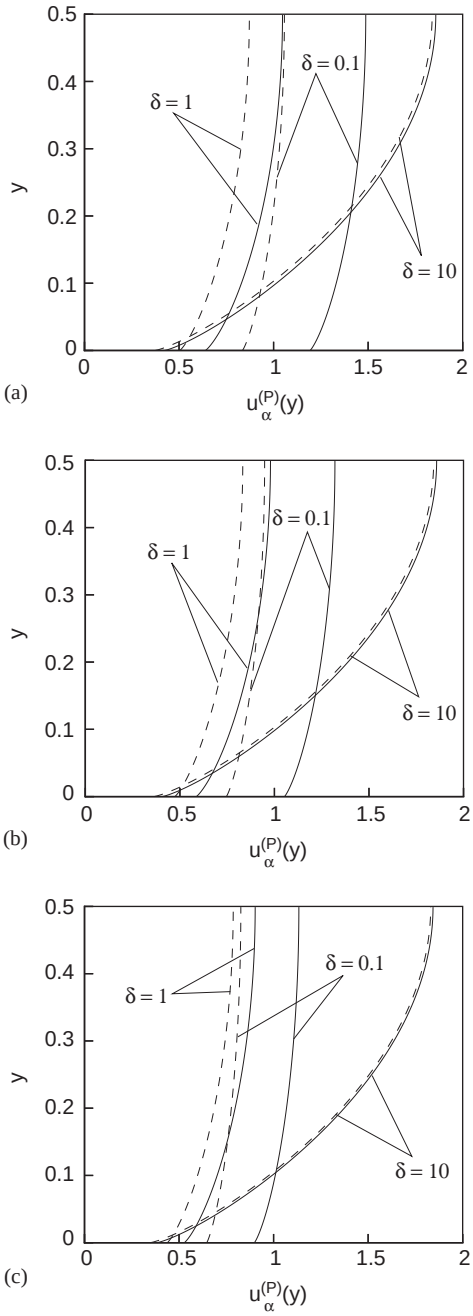

Fig. 2. Velocity profiles $u_\alpha^{(P)}(y)$ of each species of the Ne–Ar mixture (solid line—Ne, dashed line—Ar) due to a pressure gradient for realistic potential and various values of δ: (a) $C_0 = 0.1$; (b) $C_0 = 0.5$; (c) $C_0 = 0.9$.

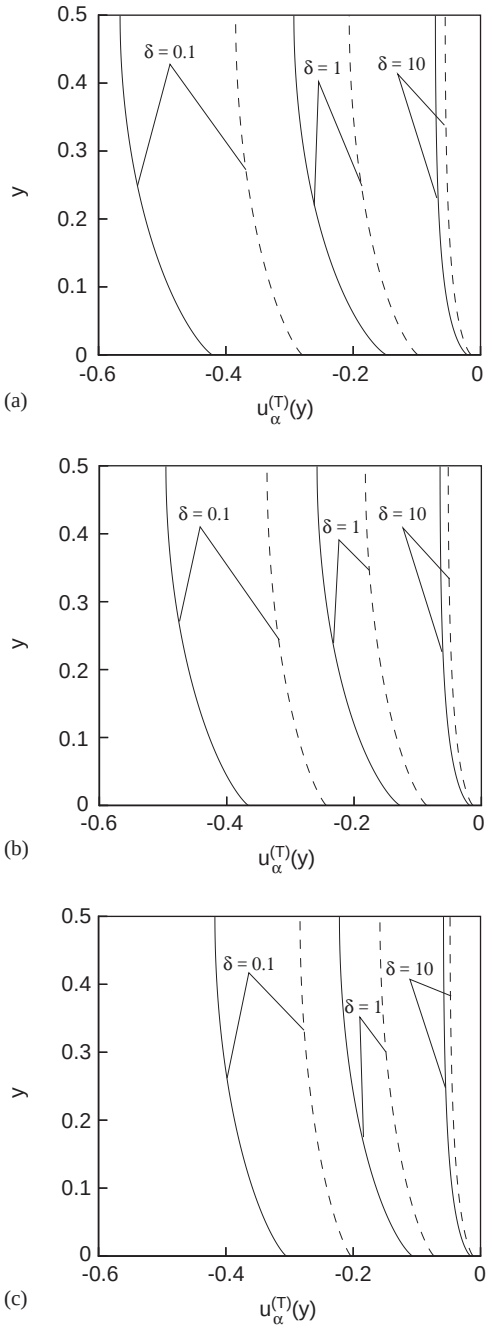

Fig. 3. Velocity profiles $u_\alpha^{(T)}(y)$ of each species of the Ne–Ar mixture (solid line—Ne, dashed line—Ar) due to a temperature gradient for realistic potential and various values of δ: (a) $C_0 = 0.1$; (b) $C_0 = 0.5$; (c) $C_0 = 0.9$.

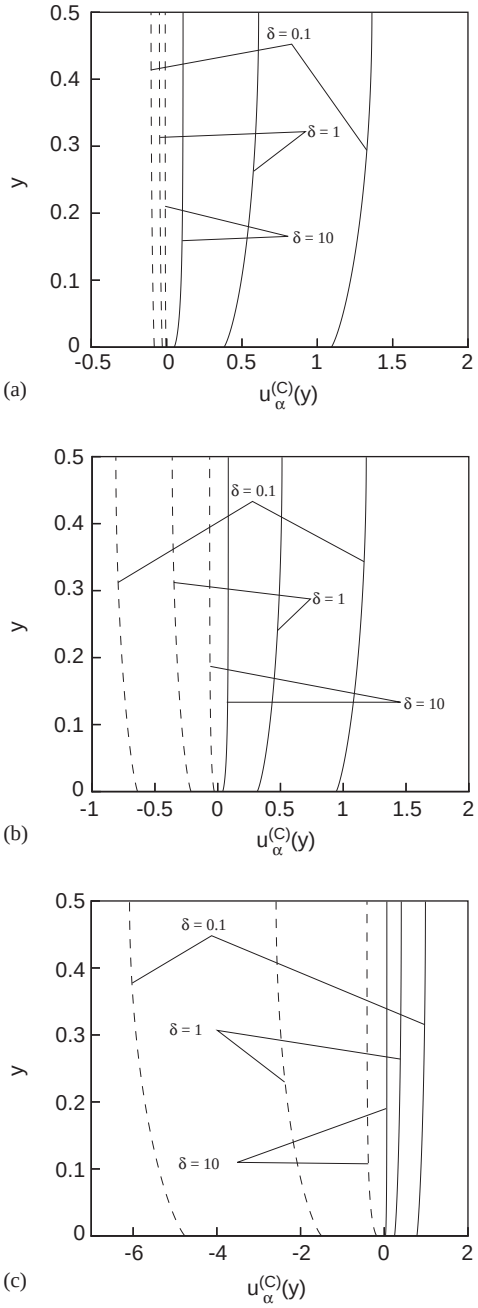

Fig. 4. Velocity profiles $u_\alpha^{(C)}(y)$ of each species of the Ne–Ar mixture (solid line—Ne, dashed line—Ar) due to a concentration gradient for realistic potential and various values of δ: (a) $C_0 = 0.1$; (b) $C_0 = 0.5$; (c) $C_0 = 0.9$.

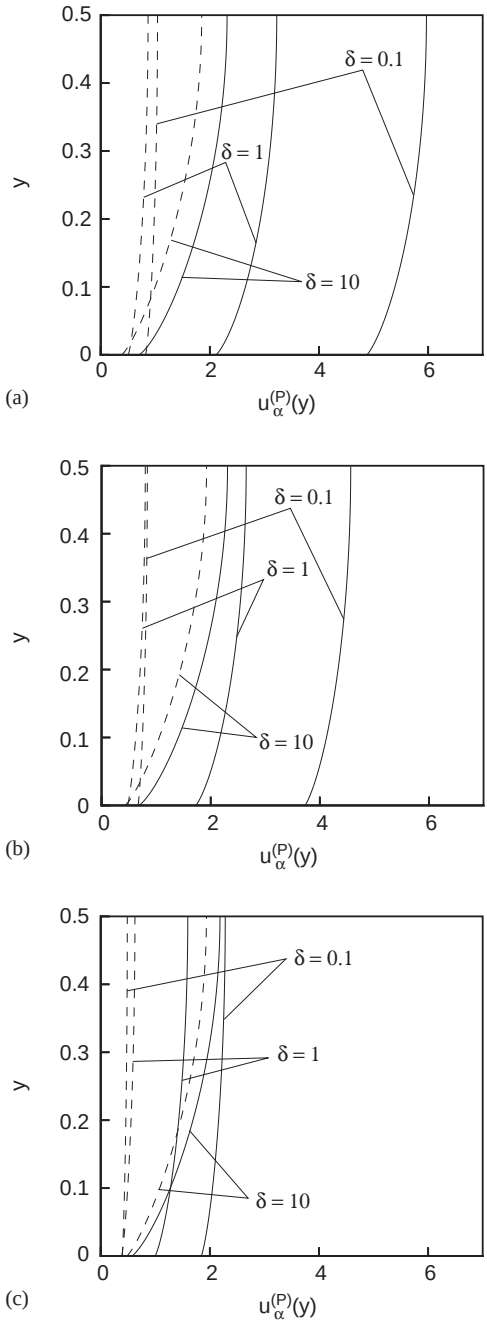

Fig. 5. Velocity profiles $u_\alpha^{(P)}(y)$ of each species of the He–Xe mixture (solid line—He, dashed line—Xe), due to a pressure gradient for realistic potential and various values of δ: (a) $C_0 = 0.1$; (b) $C_0 = 0.5$; (c) $C_0 = 0.9$.

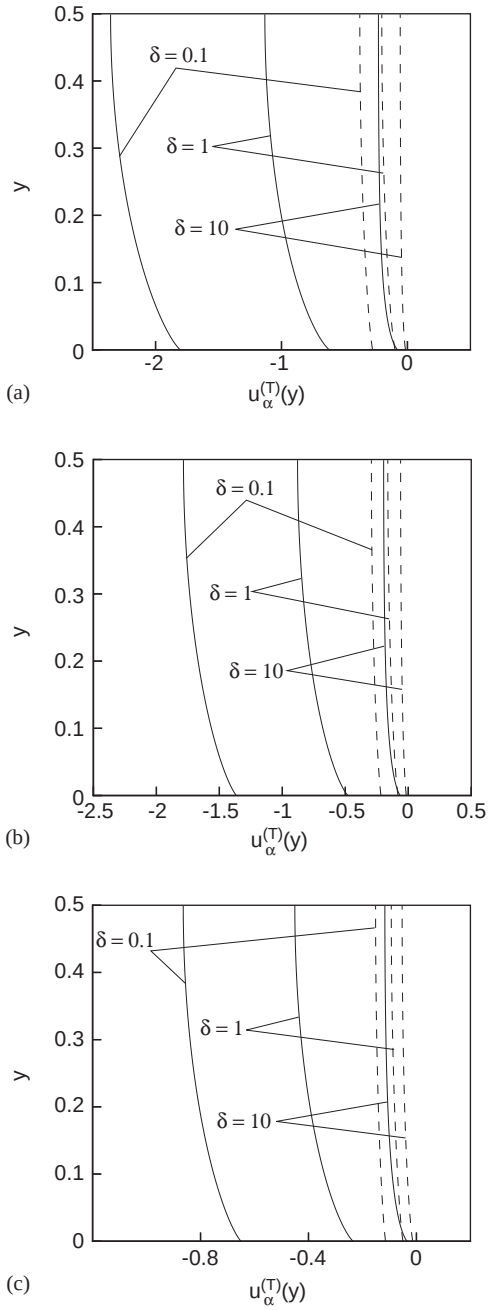

Fig. 6. Velocity profiles $u_x^{(T)}(y)$ of each species of the He–Xe mixture (solid line—He, dashed line—Xe), due to a temperature gradient for realistic potential and various values of δ: (a) $C_0 = 0.1$; (b) $C_0 = 0.5$; (c) $C_0 = 0.9$.

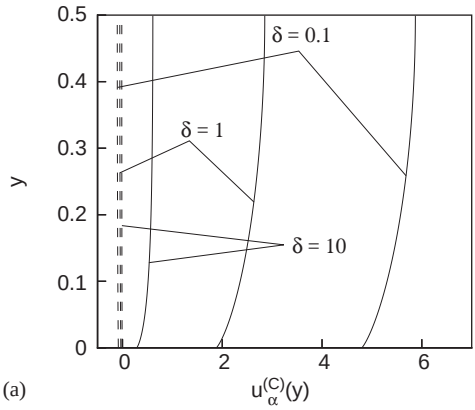

(a)

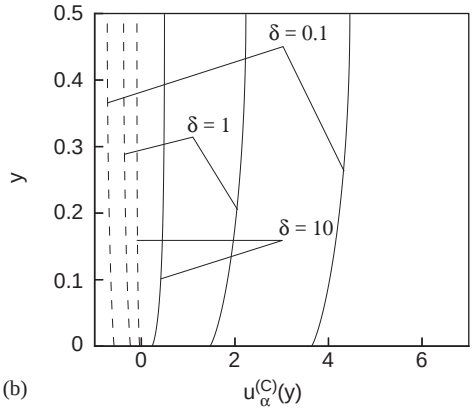

(b)

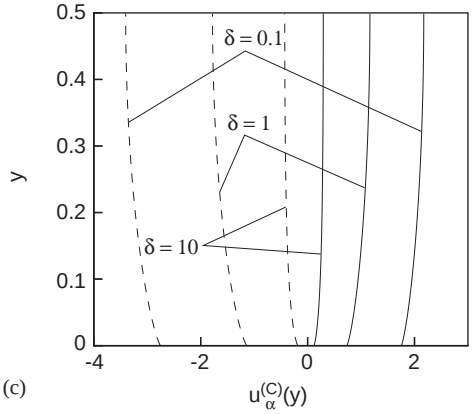

(c)

Fig. 7. Velocity profile $u_\alpha^{(C)}(y)$ of each species of the He–Xe mixture (solid line—He, dashed line—Xe), due to a concentration gradient for realistic potential and various values of δ: (a) $C_0 = 0.1$; (b) $C_0 = 0.5$; (c) $C_0 = 0.9$.

Appendix A. Basic elements of the McCormack linearized collision term

The McCormack linearized collision term [19] for the flow problems under investigation reads

$$L_{\alpha\beta}h_\alpha = -\gamma_{\alpha\beta}h_\alpha + 2\sqrt{\frac{m_\alpha}{m}}\left[\gamma_{\alpha\beta}u_\alpha - \nu^{(1)}_{\alpha\beta}(u_\alpha - u_\beta) - \frac{1}{2}\,\nu^{(2)}_{\alpha\beta}\left(q_\alpha - \frac{m_\alpha}{m_\beta}\,q_\beta\right)\right]c_{\alpha x}$$
$$+ 4[(\gamma_{\alpha\beta} - \nu^{(3)}_{\alpha\beta})\Pi_\alpha + \nu^{(4)}_{\alpha\beta}\Pi_\beta]c_{\alpha x}c_{\alpha y} + \frac{4}{5}\sqrt{\frac{m_\alpha}{m}}\left[(\gamma_{\alpha\beta} - \nu^{(5)}_{\alpha\beta})q_\alpha\right.$$
$$\left. + \nu^{(6)}_{\alpha\beta}\sqrt{\frac{m_\beta}{m_\alpha}}\,q_\beta - \frac{5}{4}\,\nu^{(2)}_{\alpha\beta}(u_\alpha - u_\beta)\right]c_{\alpha x}\left(c^2_\alpha - \frac{5}{2}\right), \qquad \alpha,\beta = 1,2. \tag{A.1}$$

The collision frequencies $\gamma_\alpha = \gamma_{\alpha\alpha} + \gamma_{\alpha\beta}$ are expressed as

$$\gamma_\alpha = \frac{S_\alpha S_\beta - \nu^{(4)}_{\alpha\beta}\nu^{(4)}_{\beta\alpha}}{S_\beta + \nu^{(4)}_{\alpha\beta}}\,, \tag{A.2}$$

where

$$S_\alpha = \nu^{(3)}_{\alpha\alpha} - \nu^{(4)}_{\alpha\alpha} + \nu^{(3)}_{\alpha\beta}\,. \tag{A.3}$$

In Eqs. (A.2) and (A.3), $\alpha = 1,2$ and $\beta \neq \alpha$. In addition

$$\nu^{(1)}_{\alpha\beta} = \frac{16}{3}\,\frac{m_{\alpha\beta}}{m_\alpha}\,n_\beta\Omega^{11}_{\alpha\beta}\,, \tag{A.4}$$

$$\nu^{(2)}_{\alpha\beta} = \frac{64}{15}\left(\frac{m_{\alpha\beta}}{m_\alpha}\right)^2 n_\beta\left(\Omega^{12}_{\alpha\beta} - \frac{5}{2}\,\Omega^{22}_{\alpha\beta}\right)\,, \tag{A.5}$$

$$\nu^{(3)}_{\alpha\beta} = \frac{16}{5}\,\frac{m^2_{\alpha\beta}}{m_\alpha m_\beta}\,n_\beta\left(\frac{10}{3}\,\Omega^{11}_{\alpha\beta} + \frac{m_\beta}{m_\alpha}\,\Omega^{22}_{\alpha\beta}\right)\,, \tag{A.6}$$

$$\nu^{(4)}_{\alpha\beta} = \frac{16}{5}\,\frac{m^2_{\alpha\beta}}{m_\alpha\, m_\beta}n_\beta\left(\frac{10}{3}\,\Omega^{11}_{\alpha\beta} - \Omega^{22}_{\alpha\beta}\right)\,, \tag{A.7}$$

$$\nu^{(5)}_{\alpha\beta} = \frac{64}{15}\left(\frac{m_{\alpha\beta}}{m_\alpha}\right)^3\frac{m_\alpha}{m_\beta}\,n_\beta\left[\Omega^{22}_{\alpha\beta} + \left(\frac{15m_\alpha}{4m_\beta} + \frac{25}{8}\,\frac{m_\beta}{m_\alpha}\right)\Omega^{11}_{\alpha\beta}\right.$$
$$\left. - \frac{1}{2}\,\frac{m_\beta}{m_\alpha}(5\Omega^{12}_{\alpha\beta} - \Omega^{13}_{\alpha\beta})\right]\,, \tag{A.8}$$

$$\nu^{(6)}_{\alpha\beta} = \frac{64}{15}\left(\frac{m_{\alpha\beta}}{m_\alpha}\right)^3\left(\frac{m_\alpha}{m_\beta}\right)^{3/2} n_\beta\left[-\Omega^{22}_{\alpha\beta} + \frac{55}{8}\,\Omega^{11}_{\alpha\beta} - \frac{5}{2}\,\Omega^{12}_{\alpha\beta} + \frac{1}{2}\,\Omega^{13}_{\alpha\beta}\right]\,, \tag{A.9}$$

and

$$m_{\alpha\beta} = \frac{m_\alpha m_\beta}{(m_\alpha + m_\beta)}\,. \tag{A.10}$$

The $\Omega_{\alpha\beta}^{ij}$ are the Chapman–Cowling integrals [1], which for the rigid sphere interaction read

$$\Omega_{\alpha\beta}^{(ij)} = \frac{(j+1)!}{8}\left[1 - \frac{1+(-1)^i}{2(i+1)}\right]\left(\frac{\pi kT}{2m_{\alpha\beta}}\right)^{1/2}(d_\alpha + d_\beta)^2 \,. \tag{A.11}$$

For the realistic potential case the integrals $\Omega_{\alpha\beta}^{ij}$ are calculated from the expressions given in Ref. [41].

References

[1] J.H. Ferziger, H.G. Kaper, Mathematical Theory of Transport Processes in Gases, North-Holland, Amsterdam, 1972.
[2] C. Cercignani, The Boltzmann Equation and its Application, Springer, New York, 1988.
[3] G.A. Bird, Molecular Gas Dynamics and the Direct Simulation of Gas Flows, Oxford University Press, Oxford, 1994.
[4] F. Sharipov, V. Seleznev, Data on internal rarefied gas flows, J. Phys. Chem. Ref. Data 27 (3) (1998) 657–706.
[5] H. Lang, S. Loyalka, An exact expression for the diffusion slip velocity in a binary gas mixture, Phys. Fluids 13 (7) (1970) 1871–1873.
[6] S.K. Loyalka, Velocity slip coefficient and the diffusion slip velocity for a multicomponent gas mixture, Phys. Fluids 14 (12) (1971) 2599–2604.
[7] H. Lang, S.K. Loyalka, Diffusion slip velocity—theory and experiment, Z. Naturforsch Part A—Astrophysik, Phys. Phys. Chemie A 27 (1972) 1307–1319.
[8] Y. Onishi, On the behaviour of a slightly rarefied gas mixture over plane boundaries, Z. Angew. Math. Phys. (ZAMP) 37 (1986) 573–596.
[9] Y. Onishi, On the diffusion-slip flow of a binary gas mixture over a plane wall with imperfect accommodation, Fluid Dyn. Res. 2 (1) (1987) 35–46.
[10] L. Sirovich, Kinetic modeling of gas mixture, Phys. Fluids 5 (8) (1962) 908–918.
[11] T.F. Morse, Kinetic model equations for a gas mixture, Phys. Fluids 7 (12) (1964) 2012–2013.
[12] B.B. Hamel, Kinetic model for binary gas mixture, Phys. Fluids 8 (3) (1965) 418–425.
[13] I.N. Ivchenko, S.K. Loyalka, R.V. Tompson, Slip coefficients for binary gas mixture, J. Vac. Sci. Technol. A 15 (4) (1997) 2375–2381.
[14] I.N. Ivchenko, S.K. Loyalka, R.V. Tompson, Boundary slip phenomena in a binary gas mixture, Z. Angew. Math. Phys. 53 (1) (2002) 58–72.
[15] C.E. Siewert, D. Valougeorgis, Concise and accurate solutions to half-space binary-gas flow problems defined by the McCormack model and specular-diffuse wall conditions, Eur. J. Mech. B/Fluids 2004, to appear.
[16] F. Sharipov, D. Kalempa, Velocity slip and temperature jump coefficients for gaseous mixtures. I. Viscous slip coefficient, Phys. Fluids 15 (6) (2003) 1800–1806.
[17] F. Sharipov, D. Kalempa, Velocity slip and temperature jump coefficients for gaseous mixtures. II. Thermal slip coefficient, Phys. Fluids, to appear (2004).
[18] F. Sharipov, D. Kalempa, Velocity slip and temperature jump coefficients for gaseous mixtures. III. Diffusion slip coefficient, submitted for publication.
[19] F.J. McCormack, Construction of linearized kinetic models for gaseous mixture and molecular gases, Phys. Fluids 16 (1973) 2095–2105.
[20] S. Takata, Diffusion slip for a binary mixture of hard-sphere molecular gases: numerical analysis based on the linearized Boltzmann equation, in: T.J. Bartel, M.A. Gallis (Eds.), Rarefied Gas Dynamics, Vol. 585, 22nd International Symposium, AIP Conference Proceedings, New York, 2001, pp. 22–29.
[21] S. Takata, S. Yasuda, S. Kosuge, K. Aoki, Numerical analysis of thermal-slip and diffusion-slip flows of a binary mixture of hard-sphere molecular gases, Phys. Fluids A 15 (2003) 3745–3766.
[22] A. Beskok, G.E. Karniadakis, W. Trimmer, Rarefaction and compressibility effects in gas microflows, Trans. ASME 118 (3) (1996) 448–456.

[23] C.M. Ho, Y.C. Tai, Micro-electro-mechanical systems (mems) and fluid flows, Ann. Rev. Fluid. Mech. 30 (1998) 579–612.
[24] V.G. Chernyak, V.V. Kalinin, P.E. Suetin, The kinetic phenomena in nonisothermal motion of a binary gas mixture through a plane channel, Int. J. Heat Mass Transfer 27 (8) (1984) 1189–1196.
[25] D. Valougeorgis, Couette flow of a binary gas mixture, Phys. Fluids 31 (3) (1988) 521–524.
[26] F. Sharipov, D. Kalempa, Gaseous mixture flow through a long tube at arbitrary knudsen number, J. Vac. Sci. Technol. A 20 (3) (2002) 814–822.
[27] V. Garzó, A. Santos, J.J. Brey, A kinetic model for a multicomponent gas, Phys. Fluids A 1 (2) (1989) 380–383.
[28] Y.N. Grigoryev, S.V. Meleshko, Bobylev–Krook–Wu models for multicomponent gas mixture, Phys. Rev. Lett. 81 (1) (1998) 93–95.
[29] P. Andries, K. Aoki, B. Perthame, A consistent BGK-type model for gas mixtures, J. Stat. Phys. 106 (5/6) (2002) 993–1018.
[30] S. Naris, D. Valougeorgis, S.F, K.D, Discrete velocity modelling of gaseous mixture flows in mems, Microscale Heat Transfer, Eurotherm 75, Reims, France, 2003.
[31] S.R. De Groot, P. Mazur, Non-Equilibrium Thermodynamics, Dover Inc., New York, 1984.
[32] F. Sharipov, Onsager–Casimir reciprocity relations for open gaseous systems at arbitrary rarefaction. I, General theory for single gas, Physica A 203 (1994) 437–456.
[33] F. Sharipov, Onsager–Casimir reciprocity relations for open gaseous systems at arbitrary rarefaction. II, Application of the theory for single gas, Physica A 203 (1994) 457–485.
[34] F. Sharipov, Onsager–Casimir reciprocity relations for open gaseous systems at arbitrary rarefaction. III, Theory and its application for gaseous mixtures, Physica A 209 (1994) 457–476.
[35] E.E. Lewis, W.F. Miller Jr., Computational Methods in Neutron Transport Theory, Wiley, New York, 1984.
[36] D. Valougeorgis, S. Naris, Acceleration schemes of the discrete velocity method: gaseous flows in rectangular microchannels, SIAM J. Sci. Comp. 25 (2) (2003) 534–552.
[37] F.M. Sharipov, E.A. Subbotin, On optimization of the discrete velocity method used in rarefied gas dynamics, Z. Angew. Math. Phys. (ZAMP) 44 (1993) 572–577.
[38] D. Valougeorgis, An analytical solution of the s-model kinetic equation, Z. Angew. Math. Phys. (ZAMP) 54 (2003) 112–124.
[39] C.L. Pekeris, Solution of the boltzmann-hilbert integral equation, Proc. Natl. Acad. Sci. 41 (1955) 661–669.
[40] C.L. Pekeris, Z. Alterman, Solution of the boltzmann-hilbert integral equation. II, The coefficients of viscosity and heat conduction, Proc. Natl. Acad. Sci. 43 (1957) 998–1007.
[41] J. Kestin, K. Knierim, E.A. Mason, B. Najafi, S.T. Ro, M. Waldman, Equilibrium and transport properties of the noble gases and their mixture at low densities, J. Phys. Chem. Ref. Data 13 (1) (1984) 229–303.